Summer Student Programme 2025

Characterization and Validation of Irradiated Novel Vacuum Sensors

Adrian Huber[1,2]

[1]Experimental Physics Department, CERN, 1 Esplanade des Particules, CH-1211 Geneva 23, Switzerland

[2]University of Applied Sciences Technikum Wien, Höchstädtpl. 6, 1200 Wien, Austria

(Dated: September 10, 2025)

Abstract

The High-Luminosity Large Hadron Collider upgrade will expose vacuum systems to radiation levels ten times higher than current operations. Commercially available radiation-hard sensors cost approximately 2500 CHF per channel, making large-scale deployment prohibitively expensive. This study evaluates low-cost thermopile-based Pirani gauges as alternatives for vacuum monitoring in radiation environments. A test setup was constructed with dual-pump vacuum system, custom feedthrough connections, and differential voltage readout for sensors operating from 10^3 to 10^{-3} mbar. Individual sensor characterization revealed significant unit-to-unit variability, requiring separate baseline establishment. Radiation exposure testing at CERN's CHARM facility covered three dose levels: 38 Gy, 551 Gy, and 1500 Gy. Post-irradiation evaluation of the first two batches demonstrated remarkable radiation tolerance, with drift effects remaining well within the manufacturer's reproducibility specification. Observed drift magnitudes were minimal and need to be confirmed at higher radiation exposure. These results indicate that low-cost thermopile sensors represent a promising cost-effective solution for HL-LHC vacuum monitoring, enabling higher granularity monitoring and improved redundancy.

Acknowledgements

Supervision was provided by Sune Jakobsen (EP-DT-TP), Valentina Reynaud (EP-DT-DI), Maciej Ostrega (EP-DT-DI), and Xavier Pons (EP-DT-DI). Additional contributions were made by Miranda Van Stenis (EP-DT-EF), Wil Vollenberg (TE-VSC-SCC), and Marc Carrichon and Bayram Dinger (DI Workshop).

I Introduction

The High-Luminosity Large Hadron Collider (HL-LHC) upgrade will expose vacuum systems to radiation levels ten times higher than current operations [1]. This increase necessitates radiation-tolerant vacuum sensors for reliable detector performance. However, commercially available radiation-hard sensors cost approximately 2500 CHF per channel including readout electronics [2], making large-scale deployment prohibitively expensive. Previous cost-reduction efforts involved relocating readout electronics to low-radiation areas while keeping sensor heads in the vacuum system [3]. Although this approach reduced radiation damage to electronics, it required extensive manual labor and offered limited cost savings.

Recently, low-cost Pirani gauges without integrated electronics have become available at a fraction of the cost. While manual labor is still required to establish the readout system, sensors can be easily swapped without modifications once the system is integrated. Unlike traditional Pirani sensors that rely on pressure-dependent resistance, these new sensors use multiple thermocouples that generate pressure-dependent voltages within the vacuum environment.

Although this price reduction would enable higher granularity monitoring and improved redundancy, the radiation tolerance of these sensors remains uncharacterized. The project addresses this knowledge gap through systematic testing: constructing a calibrated test setup, establishing baseline sensor performance, exposing sensors to controlled radiation doses, and evaluating post-irradiation characteristics.

II Test Setup

To characterize the sensors, a precise test setup is needed. Building this test setup was an iterative process and included a vacuum system and the corresponding readout to the sensors.

A Vacuum Setup

The vacuum system was designed to achieve high vacuum levels with precise pressure control and reproducible pumping rates. The system architecture enables systematic characterization of multiple sensors under identical conditions.

The pumping configuration consists of a dual-pump unit that provides the primary vacuum generation capability. Pressure regulation is achieved through two valves arranged in series, allowing precise adjustment of pressure levels and controlled modification of pumping rates during operation. To maintain stable pressure distribution throughout the system, a gas volume was inserted to balance pressure fluctuations across all measurement points.

The sensor mounting arrangement utilizes a manifold with additional crosses to accommodate simultaneous testing of six Pirani sensors. Three reference sensors provide precise, unified pressure measurements that serve as calibration standards for comparison with test sensors. This configuration ensures statistical reliability while maintaining measurement accuracy across the entire pressure range. Figure 1 shows the schematic of the vacuum setup.

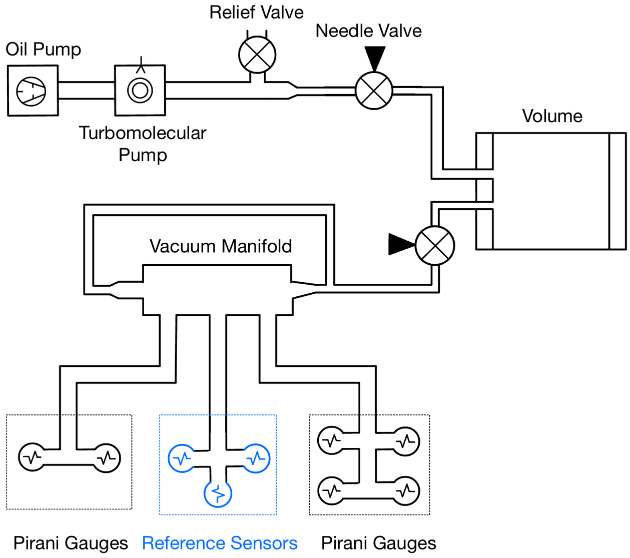

Figure 1: Complete vacuum setup configuration showing the interconnection of pumping, regulation, and measurement components.

B Cables and Connectors

Custom cables and corresponding connections were manufactured for the test setup. The custom cables from the readout system to the feedthrough connection were manufactured by the Detector Interface (DI) Workshop. For the feedthrough, a hole was drilled into a KF16 blind flange made of aluminum, and the corresponding connectors for the sensors were purchased and assembled by the Engineering Facilities (EF) section. To facilitate easier switching between sensors, pin headers were soldered onto the connectors facing the vacuum side. Cables with polyimide coating were used to minimize outgassing.

C Readout System

The readout system exploits the thermoelectric effect in thermopile sensors, where temperature differences generate measurable voltages proportional to the vacuum pressure. The thermopile sensors require a 1.2 V excitation voltage supplied to a resistive heater that elevates the temperature of the thermocouples. This resistive heater dissipates power, with heat loss through gas conduction being directly proportional to pressure.

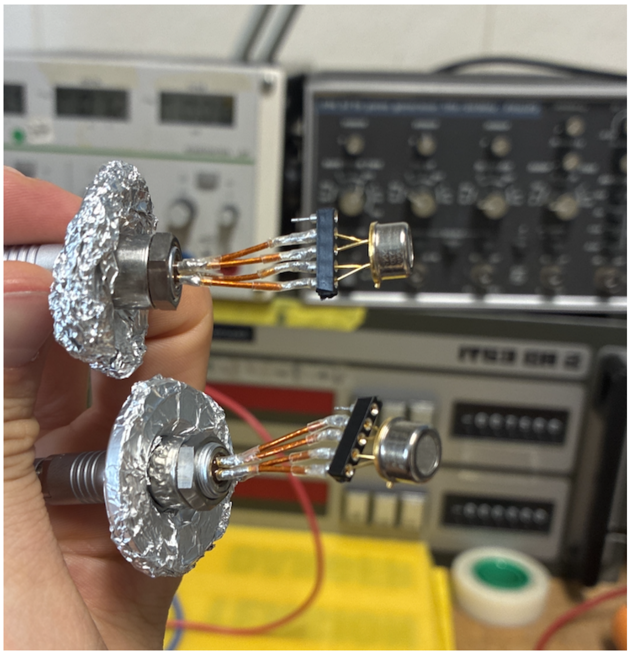

Figure 2: Assembled feedthrough connection for the test sensors. The modified blind flange is still wrapped in Aluminium foil to preserve the cleanliness.

The measurement principle relies on the thermopile's ability to detect temperature differences between the heated membrane and the cold substrate using the Seebeck effect. The output voltage is proportional to this temperature differential, which increases at lower pressures due to reduced heat loss, resulting in a characteristic nonlinear S-shaped response curve [5].

Hardware implementation centers on the NI 9205 data acquisition module operating in differential mode for analog voltage acquisition. Supply voltages are provided separately for both reference and test sensors to ensure measurement independence. Since the excitation voltage directly influences the thermopile's voltage output, continuous monitoring and storage of supply voltage values is essential for accurate pressure conversion.

The data acquisition system employs a custom LabVIEW program that handles real-time channel selection, differential voltage measurement, and system parameter monitoring. A Python integration module performs voltage-to-pressure conversion based on manufacturer calibration data [5] and generates live pressure displays. The system continuously logs all relevant parameters including timestamps, channel identifiers, measured voltages, calculated pressures, standard deviations, and supply voltages to a database file for subsequent analysis.

III Characterisation of Test Sensor

The test sensor is designed to operate effectively within low to mid-vacuum levels and has a pressure range from 10^3 to 10^{-3} mbar. Achieving accurate characterization across this entire range was critical to validate sensor performance. The reference sensors, which combine multiple vacuum measurement principles, provide precise measurements from 10^3 to 10^{-8} mbar, serving as reliable calibration standards. During test runs, defined valve positions were experimentally determined and adjusted to ensure smooth pumping operation while maintaining consistent environmental parameters, such as temperature. To enhance confidence in the measurement results, the functionality of the sensors was verified through multiple test runs. Each test run involved slowly pumping the system down to 10^{-3} mbar across nine distinct valve positions, followed by controlled venting. To eliminate potential influences from slight pressure variations within the setup, the sensor positions were fixed and documented. Figure 3 illustrates the time-pressure profile of a single test run, with the reference sensors demonstrating close agreement (within 5 % difference), confirming their factory-calibrated accuracy. Notably, the test sensor exhibited significant variability in its response. Since the Sensors share the same supply voltage and identical cable lengths, this variability is attributed to the sensor itself rather than external factors.

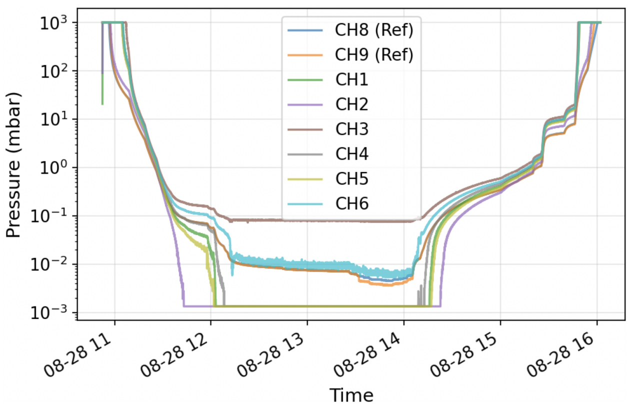

Figure 3: Pressure over time for one test round, which includes pumping the system down and venting it again. The voltage-pressure conversion of the test sensors (CH1-CH6) is based on the manufacturer calibration data.

irradiation evaluation, it is critical that each sensor delivers accurate and reproducible measurements. Figure 5 demonstrates that this requirement is satisfied, showing consistent sensor performance across multiple test runs.

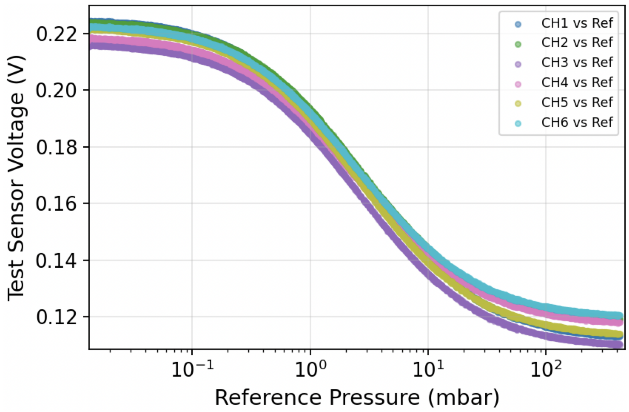

Figure 4: Voltage output of test sensors versus pressure values from reference sensors for a single test run, with data aligned by timestamps.

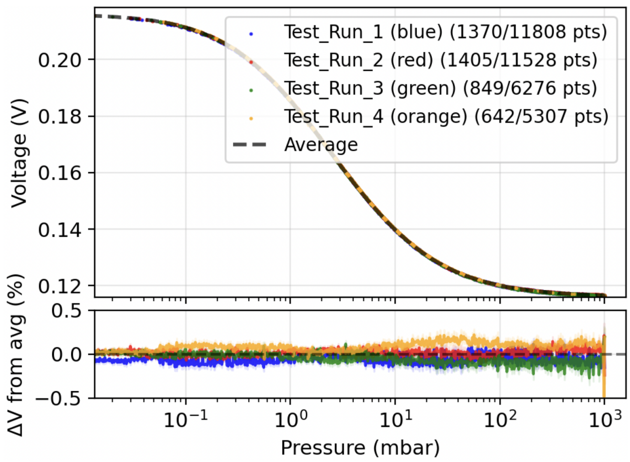

Figure 5: Repeatability measurements showing sensor stability over multiple test rounds. Nearby datapoints of the same test run were filtered out in order to increase the visibility.

A Voltage-Pressure Conversion

A central objective of sensor characterization was to reconstruct and validate the voltage-pressure relationship specified in the datasheet. As noted in Figure 3, the thermopile sensors exhibit significant variations in pressure readings despite identical conversion methods and consistent environmental parameters. These differences stem from distinct voltage outputs of individual thermopiles. Figure 4 illustrates the voltage output of the test sensors plotted against the pressure values from the reference sensors, with data points aligned by timestamps. This graph confirms that each sensor produces a unique response, necessitating individual characterization for precise results. For post-

B Baseline Creation

The final step in sensor characterization involves establishing normal operational parameters for each individual sensor. Building upon insights from the voltage-pressure relationship analysis, a baseline was created to define acceptable performance boundaries for post-irradiation comparison. The baseline uses a pressure-binning approach to handle the wide measurement range effectively. The analysis creates a logarithmically-spaced pressure grid from 10^{-3} to 10^3 mbar with a total of 10^{-3} bins. This provides uniform resolution across the log scale, which is essential given the sensors' nonlinear response characteristics. Data from at least four separate test rounds ensures statistical reliability. Each voltage-pressure measurement pair gets assigned to the appropriate pressure bin based on its reference pressure value. For each bin containing data, the analysis calculates the mean voltage, standard deviation, and counts the number of data points. Missing values in pressure bins without direct measurements are interpolated linearly between neighboring bins with data. This creates smooth baseline curves across the entire measurement range while preserving the statistical integrity of the actual measurements. The resulting baseline provides a robust reference for detecting radiation-induced changes during post-irradiation evaluation.

IV Radiation Exposure

Radiation exposure testing was performed at CERN's CHARM (CERN High energy AcceleRator Mixed field) facility [7]. The facility operates by directing a high-energy proton beam onto a target, which generates mixed radiation fields that accurately reproduce the conditions expected in the HL-LHC environment. The CHARM facility was selected for this study because it provides the precise radiation control required for systematic sensor evaluation under realistic operational conditions.

The experimental approach involved organizing sensors into batches to assess performance across different radiation levels. Three batches were prepared, each containing six well-characterized thermopile sensors. This number of sensors per batch was chosen to provide sufficient data for statistical analysis while accounting for manufacturing variations between individual units. The batch structure also allows for direct comparison of radiation effects at different dose levels.

The three batches were exposed to progressively higher radiation levels to cover dose ranges relevant to various LHC locations. This approach allows construction of dose-response curves and identification of performance degradation thresholds. Table 1 presents the detailed exposure parameters for each batch, including the total ionizing dose (TID) and neutron fluence equivalent values.

Table 1: Radiation exposure batches with corresponding dose levels and exposure durations

Batch	Sensors	Duration	Radiation Level
1	6	1 week	38 Gy, 8.5E11 1MeVeqN/cm^2
2	6	1 week	551 Gy, 4.2E12 1MeVeqN/cm^2
3	6	3 weeks	1500 Gy, 8.1E12 1MeVeqN/cm^2

The current exposure program represents the initial phase of the radiation tolerance evaluation. Additional batches are planned for exposure to even higher radiation doses, which will extend the characterization range and determine the ultimate operational limits of these sensors.

V Evaluation

Radiation damage effects in vacuum sensors are difficult to predict due to the complex interaction between radiation and sensor materials. The sensors could experience various types of performance changes, including voltage drift, noise increases, or shifts in their operational range. To detect these potential changes systematically, the evaluation analyzes different types of performance variations across the full measurement spectrum.

A Method

The evaluation of irradiated sensors repeats the same baseline creation method used for pre-radiation characterization. Post-radiation baseline data was collected using identical test procedures, measurement parameters, and statistical analysis methods. This approach ensures direct comparability between pre- and post-radiation performance. With both baselines established, systematic comparison of sensor performance becomes possible. The analysis focuses on identifying specific types of radiation damage and quantifying their magnitude relative to the sensors' specified accuracy tolerances. The difference analysis processes pre- and post-irradiation datasets using identical pressure grids, enabling direct comparison at matching pressure points. For each pressure bin, the analysis calculates the percentage differences of the mean values relative to the pre-irradiation baseline. Furthermore, the uncertainty propagation combines uncertainties from both datasets using standard error propagation methods. The combined uncertainty equals the square root of the sum of squared uncertainties from pre- and post-irradiation measurements.

B Results

The current evaluation covers Batch 1 (38 Gy, 8.5E11 1MeVeqN/cm^2) and Batch 2 (551 Gy, 4.2E12 1MeVeqN/cm^2), both of which have completed post-radiation testing. Batch 3, exposed to 1500 Gy and 8.1E12 1MeVeqN/cm^2, remains scheduled for evaluation following completion of the extended three-week exposure period. The results in Figure 6 show the comparison of a sensor response before and after 38 Gy radiation exposure across the complete operational range. Figure 7 combines the difference plots of multiple sensors from this batch, the average of these differences is calculated and displayed at the bottom (blue chart). The 551 Gy exposure results are presented in Figure 8. Figure 9 also displays multiple difference plots of this batch, with the resulting average shown in blue at the bottom.

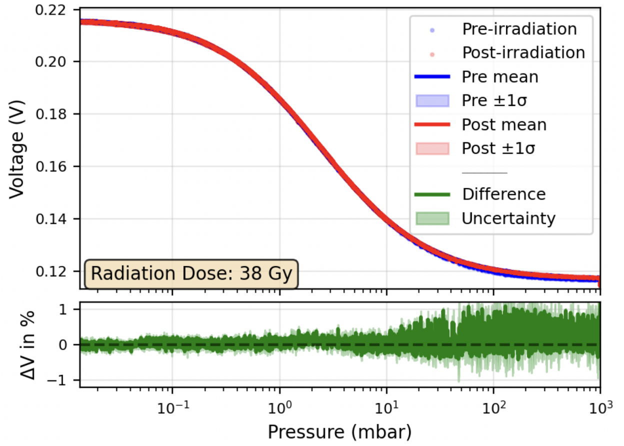

Figure 6: Pre- and post-irradiation response of a sensor after 38 Gy exposure across the operational range including the relative difference in Percentage.

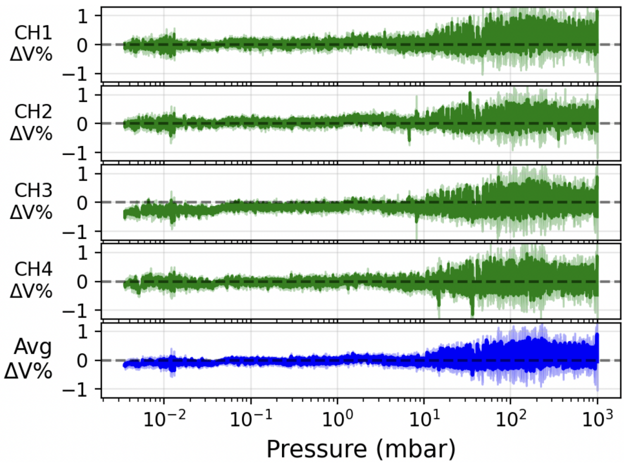

Figure 7: Difference plots of multiple sensors from the 38 Gy exposure batch and the resulting average in blue.

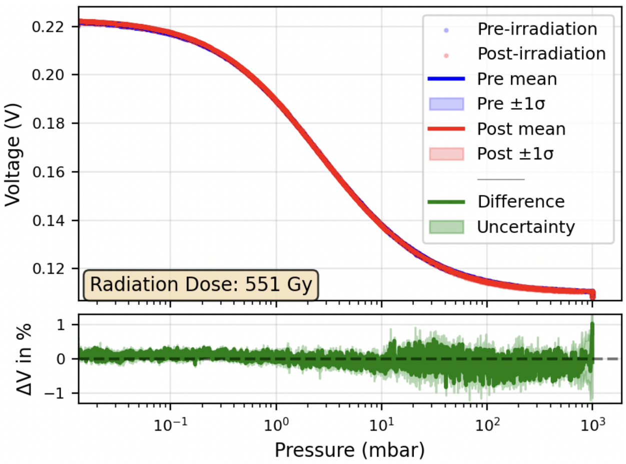

Figure 8: Pre- and post-irradiation response of a sensor after 551 Gy exposure across the operational range including the relative difference in Percentage.

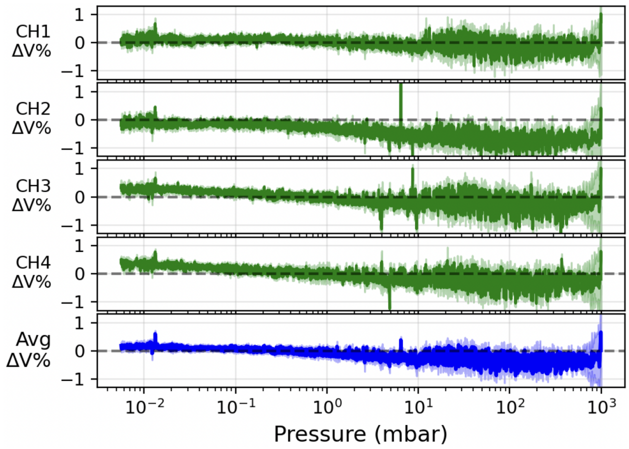

Figure 9: Difference plots of multiple sensors from the 551 Gy exposure batch and the resulting average in blue.

VI Conclusion

Analysis of the evaluated batches reveals that the thermopile sensors show remarkable radiation tolerance at the tested dose levels. Both the 38 Gy and 551 Gy batches show minimal deviation from their pre-radiation performance characteristics, with no clear evidence of systematic radiation-induced degradation.

A noticeable increase in noise appears for pressure values above 100 mbar, but this is likely attributed to the reference sensors rather than radiation effects. While the reference sensor's upper limit is set at 10^3 mbar, its 5% reproducibility specification only extends to 100 mbar. The datasheet provides no reproducibility values for the remaining range [6].

The difference plots from the 551 Gy exposure in Figure 9 suggest possible minor non-linear drift effects. The average difference plot shows a pressure-dependent drift of approximately 0.7% across the low-noise measurement range (10^{-2} to 10 mbar). However, these potential changes remain well within the reproducibility specification provided in the manufacturer's datasheet. Additionally, this effect could be partially attributed to analog-to-digital conversion limitations. The 30 µV resolution contributes approximately 0.03% uncertainty at the lower voltage range (0.12 V) and 0.01% at the higher range (0.22 V). Since the test sensors rely on the Seebeck effect, even small temperature changes in the environment could further effect the results.

The data shows no signs of noise increase or changes in the operating range due to radiation exposure. This makes the sensors suitable for applications like leak detection, where only relative changes need to be measured. For applications requiring high-precision vacuum measurements, the non-linear drift needs confirmation through higher radiation dose testing. The magnitude of any drift must then be evaluated individually for each application to determine if it falls within acceptable tolerances.

References

[1] CERN, "High-Luminosity LHC: Increasing the LHC's performance," https://home.web.cern.ch/press/2022/HL-LHC (2022).

[2] CERN Internal Collaboration, "HL-LHC Radiation Levels Project Report," Internal Document, CERN (2024).

[3] F. Faccio, G. Blanchot, A. Dabrowski, S. Detraz, S. Michelis, J. Troska, and L. Olantera, "Radiation-Tolerant Electronics for the HL-LHC Vacuum Systems," https://indico.cern.ch/event/697988/papers/3056160/files/8247-Paper_TWEPP18_RadTol_Electronics_Vacuum_26-12-2018.pdf (2018).

[4] Xu, S.; Zhou, N.; Shi, M.; Zhang, C.; Chen, D.; Mao, H., "Overview of the MEMS Pirani Sensors" https://doi.org/10.3390/mi13060945 (2022).

[5] Posifa Technologies, "PVC3000 Series Vacuum Sensor Datasheet," https://posifatech.com/wp-content/uploads/2022/03/Datasheet_PVC3000_Vacuum_RevC_C12.pdf (2022).

[6] Pfeiffer Vacuum, "PKR 251 Compact FullRange Gauge, FPM sealed Operating Instructions," https://edg.uchicago.edu/tutorials/pumps/BG5155BEN.pdf (2011).

[7] CERN, "CHARM: CERN High energy AcceleRator Mixed field facility," https://r2e.web.cern.ch/about-radiation/test-facilities/charm (n.d.).